

## Experimental modeling of antimony sulfides-rich geothermal deposits and their solubility in the presence of polymeric antiscalants

Emre Karaburun<sup>a</sup>, Yigit Sozen<sup>b</sup>, Celal Çiftçi<sup>c</sup>, Hasan Sahin<sup>b</sup>, Alper Baba<sup>d</sup>, Ümit Akbey<sup>e</sup>, Mehmet İrfan Yeşilnacar<sup>f</sup>, Eray Erdim<sup>g</sup>, Simona Regenspurg<sup>h</sup>, Mustafa M. Demir<sup>a,\*</sup>

<sup>a</sup> Department of Materials Science and Engineering, İzmir Institute of Technology, Gülbahçe, Urla, İzmir 35430, Turkey

<sup>b</sup> Department of Photonics, İzmir Institute of Technology, Gülbahçe, Urla, İzmir 35430, Turkey

<sup>c</sup> Graduate School of Natural and Applied Sciences, Renewable Energy Resources/Technologies, Harran University, Şanlıurfa 63050, Turkey

<sup>d</sup> Department of International Water Resources, İzmir Institute of Technology, Gülbahçe, Urla, İzmir 35430, Turkey

<sup>e</sup> Radboud University IMM / Magnetic Resonance Research Center, Nijmegen 6500 GL, the Netherlands

<sup>f</sup> Department of Environmental Engineering, Harran University, Osmanbey Campus, Haliliye, Şanlıurfa 63050, Turkey

<sup>g</sup> NEU CHEMIE, Istanbul Leather Industrial Zone, Tuzla 34597, Turkey

<sup>h</sup> German Research Center for Geosciences, Helmholtz-Zentrum GFZ Potsdam, Germany

### ARTICLE INFO

#### Keywords:

Geothermal deposits  
Antimony sulfide  
Scaling  
Stibnite  
Inhibitor

### ABSTRACT

Antimony (Sb)-rich geothermal deposits have been observed in many geothermal power plants worldwide. They occur as red-colored, sulfidic precipitates disturbing energy-harvesting by clogging the geothermal installations. In order to prevent the formation of this scale, information on its physicochemical features is needed. For this purpose, Sb-rich sulfide-based deposits were synthesized at controlled conditions in a pressurized glass reactor at geothermal conditions (135 °C and 3.5 bar). Various polymeric antiscalants with different functional groups, such as acrylic acid, sulphonic acid, and phosphonic acid groups were tested for their effect on Sb sulfide solubility. An additional computational study was performed to determine the binding energy of Sb and S atoms to these groups. The results suggest that sulfonic acid groups are the most affective. Therefore, it was concluded that these macromolecule containing sulfonic acid groups and poly (vinyl sulfonic acid) derivatives could potentially act as antiscalants for the formation of antimony sulfide.

### 1. Introduction

Scaling along the pipeline is a critical issue in geothermal power plants since its removal causes high maintenance time and thus an economic loss (Azaroual et al., 2004; Baba et al., 2015; Ellis and Mahon, 1977; Reyes et al., 2002). The precipitation of solid colloidal substances on all surfaces of the system dramatically reduces energy harvesting and the removal of the deposit is tedious and requires a huge effort. The composition of most deposits in geothermal power plants of high enthalpy geothermal regions is mainly carbonates and silicates. Antimony-rich sulfide deposits have recently also appeared in several geothermal plants, including those with low, medium, and high enthalpy fluids (Williams-Jones and Nobmand, 1997). The formation process of the deposits differs from those of carbonates and silicates, since antimony is a metalloid, which can be readily dissolved and transported by the hydrothermal fluid due to changes in pH,

temperature, and aqueous sulfide concentration within faults and fractures of the geological formation, especially in fault-crack controlled systems (Hofstra et al., 2013). Stibnite is an antimony-sulfide mineral with a system of an orthorhombic crystal lattice. Stibnite is mainly formed in veins, coarse-grained lithology, and breccias that can be found in the fault zone of sedimentary and metasedimentary but also serpentinized mafic and ultramafic rocks. Some stibnite is disseminated in carbonate-altered rocks surrounding the fault zone. Massive stibnite-pyrite replacements, which may form pods or lenses up to tens of meters long, are relatively uncommon but are sources of a rich ore (Andre, 1996). Stibnite occurs in various deposits, including epithermal veins, pegmatites, replacements, and hydrothermal deposits (Miller, 1973).

In natural geothermal systems, antimony usually occurs bound to sulfides as a trisulfide,  $Sb^{3+}$  (Çiçek, 2020; Stauffer and Thompson, 1984). Stibnite ( $Sb_2S_3$ ), known as antimony trisulfide. Crystalline stibnite is soft

\* Corresponding author.

E-mail address: [mdemir@iyte.edu.tr](mailto:mdemir@iyte.edu.tr) (M.M. Demir).

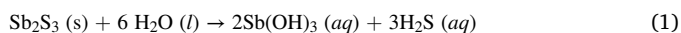
<https://doi.org/10.1016/j.geothermics.2022.102452>

Received 21 November 2021; Received in revised form 1 May 2022; Accepted 7 May 2022

Available online 13 May 2022

0375-6505/© 2022 Elsevier Ltd. All rights reserved.

and has a density of 4.63 g·mL<sup>-1</sup>. The melting point is 550 °C. It occurs naturally as a mineral that forms typically acicular (needle-like) black crystals. In hydrothermal systems, solubility of stibnite is very sensitive to temperature and variation of pH. Stibnite dissolves in water in the form of hydroxide, and as the formation of stibnite increases, the hydrogen sulfide concentration increases. This reaction can be expressed simply by the following equation (Brown, 2011):



In an aqueous solution of Sb-containing salts, antimony does not occur as the free cation (Sb<sup>3+</sup>) unless the medium is highly acidic. Since antimony has two valences (III or IV), it forms many different molecular species. For instance, the interaction of Sb<sub>2</sub>S<sub>3</sub> with H<sub>2</sub>S, given in Eq. (2), yields sulfide salts of antimony:



Antimony also has an oxidized form with a valence of +5. It forms by a slow oxidation of Sb (III) compounds. In aqueous systems, the oxidized Sb (V) species eventually turns into Sb (OH)<sub>6</sub> (Brown, 2011).

Stibnite scaling has been observed in New Zealand, Italy, USA, Indonesia, and El Salvador so far (Wilson et al., 2007). In the past two years, stibnite scaling has also increased in power plants due to the widespread application of binary cycle power plants in Turkey. The chemistry of brine has remarkably changed with time. The origin of this process may be due to the fact that the brine had initially been taken from the carbonate rocks, whereas recently it is obtained from the calc-schists. This mechanism brings the minerals from the deeper part of the rocks.

Antiscalants have frequently been used to prevent the formation of deposits such as in metal silicates mitigation by polymeric molecules in aqueous systems (Demadis et al., 2006; Topçu et al., 2019, 2017). Topçu et al. reported an increased solubility of metal silicates using a copolymeric antiscalant with various functional groups. The prevention of silica/silicate has also been achieved using antiscalants with functional groups, particularly with -NH<sub>2</sub>. So far, an additive that prevents the formation of stibnite-type deposits has not been described in the literature. While potential existing antiscalants are being considered, they need to be tested by practical scientific methods. To test the performance of an antiscalant, natural deposits as obtained from geothermal sites have to be synthesized at near-natural but well-defined conditions. Previously, a simple lab reflux apparatus using similar Sb and S sources was established that simulates these conditions up to 100 °C (Çiftçi et al., 2020). A mixture of Sb oxide and sulfide was obtained, while the fabrication of the pure sulfide phase was not successful. The reason could be the limited temperature within the reflux system, where the maximum boiling temperature of the water is achieved (100 °C), whereas higher temperatures are needed for the synthesis of antimony sulfides.

In this study, a pressurized reactor is employed to adjust the temperature and pressure to the field conditions. The temperature and pressure were fixed to 135 °C and 3.5 bar, respectively, because these thermodynamic values are close to the ones of the fields in Turkey. Since the concentration of ions varies depending on pressure, it is expected to be higher in the pressurized reactor, although the initial concentration of precursor salts is identical. Organic functional groups have a strong interaction with metals and metalloids (Demir et al., 2014; Gallup, 2002; Topçu et al., 2019, 2017).

The macromolecules containing acrylic acid, sulfonic acid, acrylamide, phosphonic acid, and hydroxyl functional groups have the potential to interact with Sb and/or S atoms in aqueous systems. (Topçu et al., 2017) The antiscaling performance was studied at various dosages. The ultimate aim of this study was to (a) synthesize and characterize a stibnite-like precipitate and (b) to develop an additive that prevents or dissolves this precipitate, which can be employed in geothermal power plants.

## 2. Experimental

For the synthesis of artificial stibnite deposits, a pressurized Büchi-glasuster reactor (Büchi AG, Uster, Switzerland) was used under field conditions (135 °C and 3.5 bar). The reactor consists of three parts: the circulator, the main part, and the controlling monitor. The circulator is used for the circulation of silicon oil to increase the temperature of the reactor up to 200 °C. The silicon oil acts as a heating jacket. The reactor is the main part of the system where the reaction is carried out. The monitor shows the system parameters as measured by pH and temperature probes.

The reaction solution was mixed by a stirrer. In a typical synthesis, 103 mg (0.47 mmol) SbCl<sub>3</sub> (Sigma Aldrich) ACS reagent >99.0% and 97 mg (0.7 mmol) of Na<sub>2</sub>S•3H<sub>2</sub>O were dissolved into 130 mL and 70 mL of ultrapure water (18.2 MΩ·cm<sup>-1</sup> at 25 °C), respectively. After they were stirred for 1 h in different beakers, they were both added to the reactor. The reaction continued for about 12 h. The initial pH of the reaction solution was 5.0 and it was 5.5 after the reaction. The black crystalline product was obtained in an ice-bath. After cooling, it was centrifuged 30 min at 6000 rpm. After centrifugation, the solid product was readily removed by a decantate solvent since the product was accumulated at the bottom of the centrifugation tube (Li et al., 2003). The solid product was put into a vacuum oven at 60 °C for approximately 12 h for drying before characterization. The concentrations of the ions are determined by Inductively Coupled Plasma Emission Spectrometry (ICP-OES) (5110 Dual View; Agilent, Santa Clara, CA, USA). For the solid characterization, X-ray diffraction (XRD) was performed using a PANalytical powder diffractometer with a copper Kα [λ=1.5416 Å] tube) for the determination of the crystal structure of the precipitates. At a scan rate of 0.08° s<sup>-1</sup>, the 2θ was scanned from 10 to 80°. The precipitate particles' morphology was examined by employing a Zeiss scanning electron microscope (SEM) (300VP; Carl Zeiss, Oberkochen, Germany). The elemental composition was determined by energy dispersive X-ray spectroscopy (EDX) (AZtec, Oxford Instruments, UK). Solid-state MAS NMR experiments were performed on a 600 MHz spectrometer equipped with a 3.2 mm probe (Varian, Palo Alto, CA, USA). All experiments were performed at room temperature and 10 kHz MAS frequency without proton decoupling.

Six different polymeric molecules were employed for testing the minimization of the deposits at various dosages: poly (acrylamide-co-vinyl sulphonic acid) P(AM-co-VSA)], poly (acrylamide-co-vinyl phosphonic acid) [P(AM-co-VPA)], poly (vinyl sulfonic acid) PVSA, polyvinyl alcohol (PVA), polyvinyl sulfonic acid sodium salt (PVSA-Na), and Alginate Sodium Salt (Aa-Na). The molecular structure is given in Scheme 1.

## 3. Results and discussion

### 3.1. Formation and characterization of the deposit

Fig. 1 presents an X-ray diffractogram of the precipitates obtained at different reaction times (from 2 h to 18 h) in a pressurized reactor. The initial concentration of the precursor is 1000 ppm of Sb ion. Two hours of reaction results in the formation of a brownish precipitate with a diffraction pattern that corresponds to Sb<sub>2</sub>O<sub>3</sub>. Extending the reaction time from 4 to 8 h, the color of the precipitate turns to gray, and the diffractogram appears to be a mixture of Sb<sub>2</sub>O<sub>3</sub> and Sb<sub>2</sub>S<sub>3</sub>. When the reaction time is further extended to 12 h, the oxide phase disappears, and the orthorhombic Sb<sub>2</sub>S<sub>3</sub> (stibnite) phase merely forms. At 16 h reaction time, the sulfide phase remains unchanged (Fig. 1). The change in color of the precipitate is clearly seen in Fig. 2. The left image shows the precipitate obtained after 2 h, which refers to the oxide phase, while the right image displays the gray color of the precipitate of the sulfide phase. The elemental composition of the deposits was determined by EDX. The theoretical composition for Sb<sub>2</sub>S<sub>3</sub> gives a precise 68:32 ratio for Sb:S. The experimental results presented in Table 1 are close to this ratio;

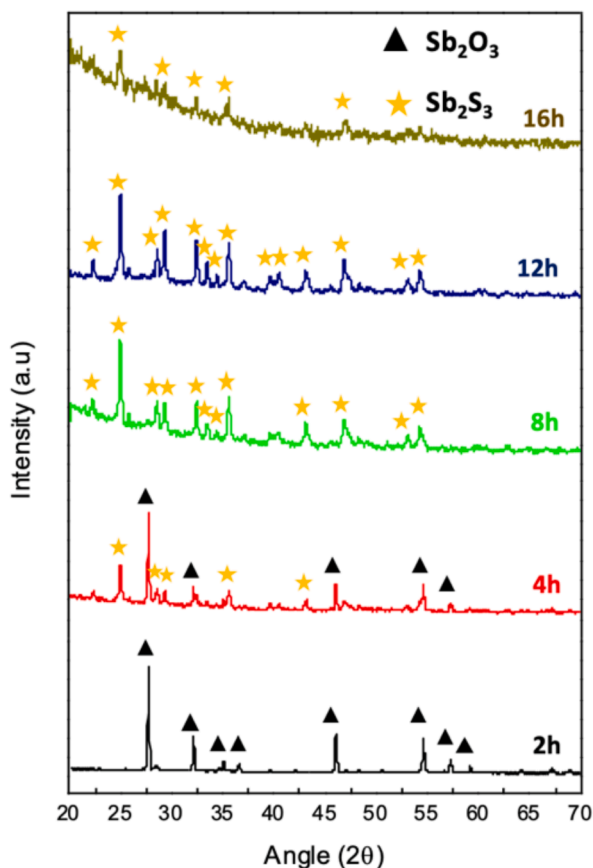


Fig. 1. XRD pattern of the precipitates prepared at different reaction times.



Fig. 2. Sb-rich precipitates obtained artificially in the lab 2 h and 12 h reaction time on filter paper.

Table 1

Elemental composition of the precipitates (% atoms) prepared at various reaction times. The composition was determined by EDX.

	Sb	S	O
Synthetic precipitate, 4 h	35	47	18
Synthetic precipitate, 8 h	31	42	26
Synthetic precipitate, 16 h	40	52	8
Theoretical ratio for $Sb_2S_3$	68	32	
Natural Precipitate	19	27	17

however, there is a small deviation from the theoretical value. The reason could be the existence of an oxide phase in the deposits (both natural and artificial ones) that reduces the percent weight of the elements.

The morphology of the artificial deposit was examined by SEM. The images are presented in Fig. 3. After a 2 h reaction, the crystals have not formed yet [not shown], while after extending the reaction time to 4 h, the crystals appear. The size of the crystals is polydisperse, with both large and small crystals. During the reaction, nucleation and growth take place simultaneously. Larger ones could be the frontiers of the crystallization process in the reaction volume, i.e., they are old crystals. On the other hand, young crystals remain small. The size of the crystals grows larger as the reaction time is extended to 8–12 h. After 16 h, small crystals appear along with the large ones. This result may suggest the occurrence of secondary nucleation in the reaction medium.

Solid-state NMR is a powerful characterization tool for determining the chemical environment of the nucleus of atoms in a molecule. In contrast to the liquid state, this method gives information concerning the native solid form of the materials studied. It has been used particularly for H and C atoms. In this study, both natural and artificial deposits were studied by solid-state  $^{121}Sb$  NMR. Only a few  $^{121}Sb$  static/MAS NMR studies have been reported so far (Faucher et al., 2014; Harmening et al., 2009). A very large electric quadrupole moment of antimony results in strong nuclear electric quadrupolar interactions even in small electric field gradient systems. This hampers the detection making it extremely difficult, resulting in the very rare observation of this nucleus mentioned, which is manifesting cubical symmetric environments. The solubilized model compound of  $^{121}Sb$  salts has a chemical shift of  $\sim 1000$  ppm, from the symmetric sites (Harmening et al., 2009). In our study, as shown in Fig. 4, independent of their nature, all samples show two signals covering a large spectral width of 2 MHz. One of the signature resonances is quite broad and appears between  $-500$  and  $800$  kHz. Another one is much more narrow and larger in signal intensity appearing at  $\sim 1250$  kHz. These signals may suggest the existence of the two different types of Sb atoms in the molecule. The former may refer to the appearance of Sb (V) atoms, while the latter may indicate the existence of Sb (III) atoms as a major component in the deposit molecules (both artificial and natural). These two different Sb sites correspond to very different chemical environments with different NMR chemical shifts and signal widths. In the course of the frequency-swept NMR experiments to cover the large spectral width, the narrow signal was always observed and the broad signal/signals disappeared rapidly at off-resonant RF irradiation. This is a clear indication of very different quadrupolar-coupling of these two sites, as a result of different chemical structures with a different symmetry around Sb nuclei. The artificial deposit seems quite similar to the natural one from the aspect of NMR spectroscopy.

### 3.2. Solubility of stibnite

The solubility of natural deposits (both in lab and in field conditions) was studied in an alkaline medium prepared by NaOH. Table 2 presents the results for the solubility of the natural deposit performed in various water solutions in the lab. Three trials were given for the parallel experiments. After a known mass of a representative deposit sample was taken, it was reacted with a 2% solution of NaOH for 1 h, and the initial and the final mass were recorded again. Mass loss was considered to be due to the dissolution of the stibnite. Most probably thioantimonite complexes are formed in the cleaning solution (Krupp, 1988). Percent mass loss was found to be nearly 90%, which serves as quite a good solubility for cleaning. The same solution composition was employed in a large volume for a geothermal power plant placed on the west coast of Turkey (Kübilay GPP). A representative decantate solution for cleaning is given in Fig. 5. The successful dissolution is observed by the change in color of the solution from colorless to orange color (which is the original color of (amorphous) stibnite).  $Sb_2S_3$  can be dissolved in alkaline solutions that are preferentially composed of NaOH and  $Na_2S$ . The reactions of  $Sb_2S_3$  with  $Na_2S$  and NaOH are shown in Eqs. (3) and Eq. (4), respectively. The reactions yield soluble species of  $Na_3SbS_3$  and  $Na_3SbO_3$ . On the other hand, NaOH has a dual function in the system.

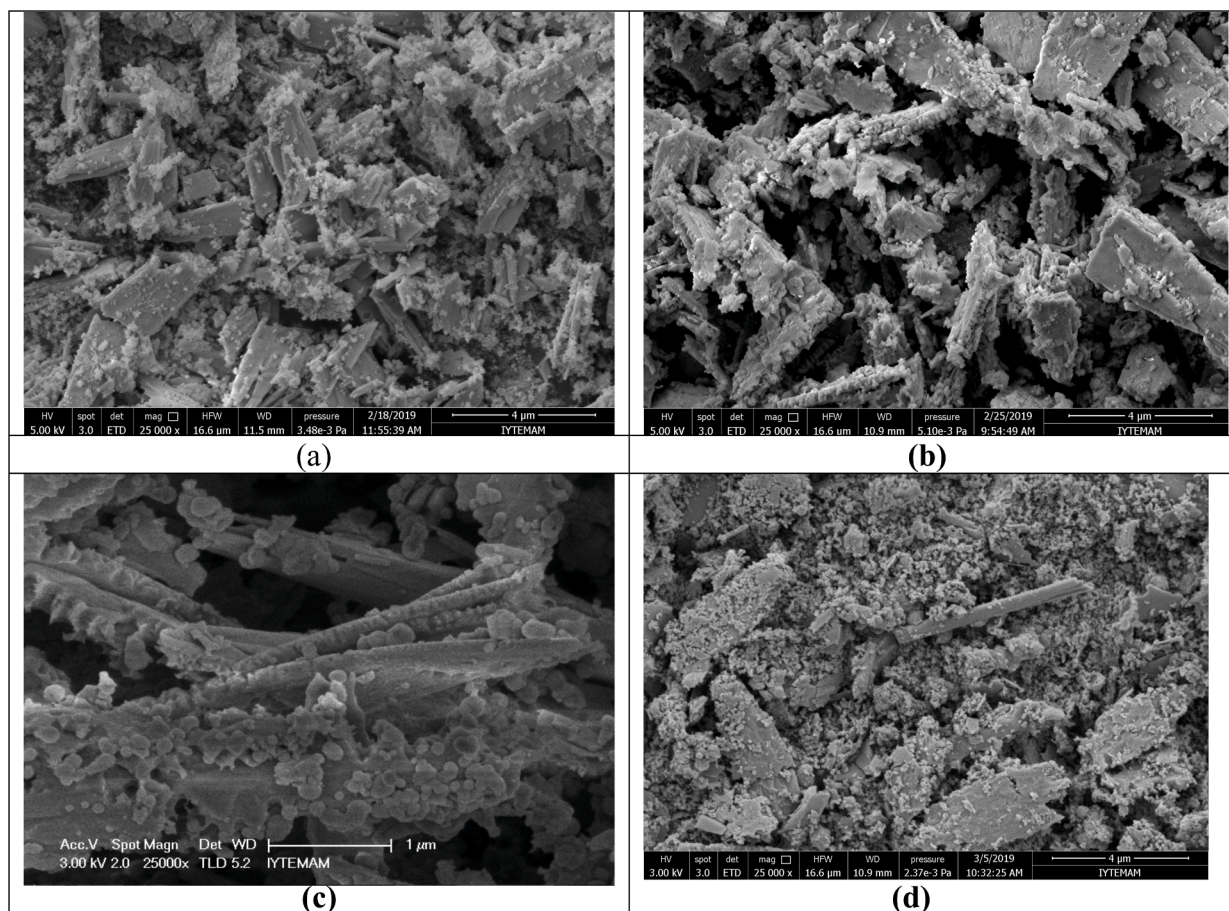


Fig. 3. SEM images of the precipitates prepared in various reaction time  $\times 25\ 000$ : (a) 4 h (b) 8 h (c) 12 h and (d) 16 h.

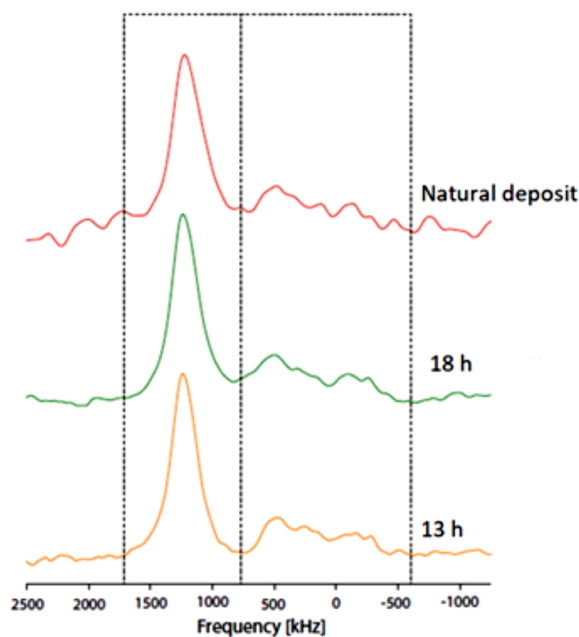


Fig. 4. Solid-state  $^{121}\text{Sb}$  MAS NMR spectra of the stibnite particles. Comparison of natural and two artificial deposits.

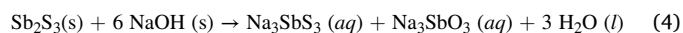
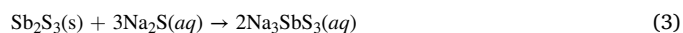
NaOH is used to prevent hydrolysis of NaHS and  $\text{H}_2\text{S}$ . An insufficient amount of the  $\text{Na}_2\text{S}$  acts as a leaching agent for the stibnite, which has a deep orange color. From the interaction of mere NaOH with  $\text{Sb}_2\text{S}_3$

Table 2

Lab-scale solubility of Sb-rich deposits in the presence of 0.5%  $\text{Na}_2\text{S}$  + 2% NaOH in water for 1 h.  $M_o$  is the initial and  $M_f$  final mass of the deposit.

Trial	$M_o$ (mg)	$M_f$ (mg)	Mass loss%
1	201.2	22.0	89.1
2	201.3	17.4	91.4
3	201.5	18.3	90.9

(without  $\text{Na}_2\text{S}$ ),  $\text{NaSbOS}$  and  $\text{NaSbS}_2$  species would be formed (Ubal dini et al., 2000; Wilson et al., 2007).



### 3.3. Performance of the antiscalants

Six water-soluble polymeric molecules were used for testing the performance of the minimization of the scale. Three of them [P(AM-co-VSA)], [P(AM-co-VPA)], and PVSA were synthesized in the laboratory (Topçu et al., 2017), while the others are commercial poly(acrylic acid), poly(vinyl alcohol), and alginate sodium salt. For testing the inhibition performance, 5, 25, 50, and 100 ppm dosages of polymeric antiscalants were introduced to the reaction medium. Fig. 6 shows the ion concentration of the ions in the presence of the antiscalants.  $\text{Sb}^{n+}$  and  $\text{S}^{2-}$  refer to Fig. 6a and 6b, respectively. The dashed line in both panels depicts the reference sample (without antiscalants). The references are 25 ppm for  $\text{Sb}^{n+}$  and 45 ppm for  $\text{S}^{2-}$ . All polymeric molecules were found

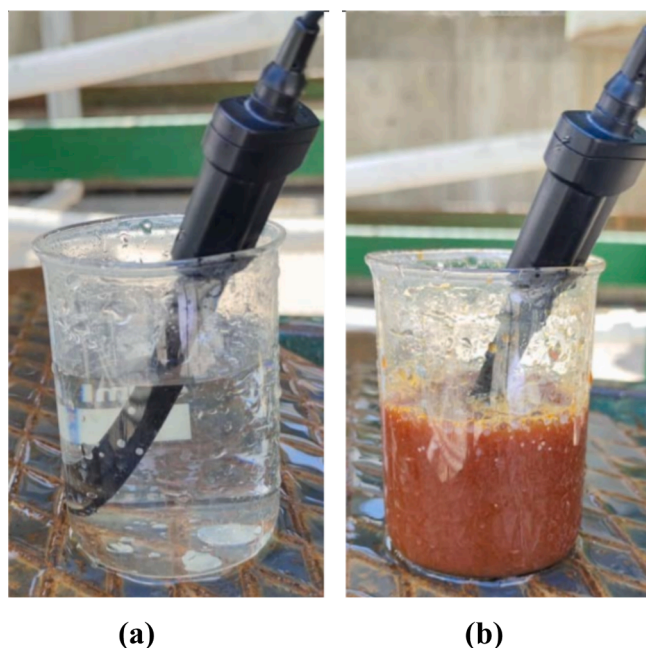


Fig. 5. Sb-rich natural deposit formed in NaOH (field results). (a) no dissolution, (b) dissolution.

to be efficient for increasing the ionic concentration of the decantate solution in terms of  $\text{Sb}^{n+}$ . ( $n=3$  or 5)

In the presence of 25 ppm of PVSA, the concentration of  $\text{Sb}^{n+}$  increased to 108 ppm. The concentration was further increased to 147 ppm at 100 ppm of P(Am-co-VSA). In particular, the molecules containing VSA increased the dissolution. The mechanism is most probably based on chelation, i.e., the interaction between the cation and the negatively charged organic ligand, which is sulfonic acid. Acrylic acid was also found to be useful in the chelation mechanism; however, it was not as effective as sulfonic acid, providing 83 ppm of  $\text{Sb}^{n+}$  at a 25 ppm dosage. On the other hand, the solubility of  $\text{S}^{2-}$  ions in the decantate solution in the presence of antiscalants has a contrasting behavior with  $\text{Sb}^{n+}$ . Its concentration is not very high compared to the reference one. It increases to 80 ppm at maximum when PVSA is employed at a dosage of 25 ppm. The usage of P(Am-co-VSA) at 100 ppm increases the concentration of  $\text{S}^{2-}$  to from 45 to 78 ppm (Fig. 6b). When the dosage is reduced to 5 ppm, the concentration of  $\text{Sb}^{n+}$  is increased for all antiscalants. This result is evidence supporting the dosage effect. For instance, it is increased to 148 ppm when PAM-co-VSA is employed, which is the maximum level of concentration achieved in this study. In fact, this argument is also valid for the solubility of  $\text{S}^{2-}$  ions. This concentration is 78 ppm, which is the highest value obtained.

There are, in fact, two mechanisms to prevent scaling: first, chelation and, second, dispersion (Topçu et al., 2017). The former mechanism involves complex formation with metal cations. Carboxylic acid, sulphonic acid, and acrylate groups are commonly used functional groups that develop chelation as already reported above. On the other hand, dispersion causes the stabilization of the colloids, i.e., the separation of the colloidal particles preventing their assembly called aggregates/agglomerates. The prevention is achieved when molecules have a polymeric nature. Antiscalants used in geothermal fields can be either monomeric or polymeric molecules. For instance, it is well established that calcium carbonate formation is prevented by the complexation with phosphate and phosphonate type molecules (chelation), which are monomeric types and of relatively small molecule size (Clearfield and Demadis, 2012). On the other hand, silicate/metal silicate deposits contain silica colloids as a constituent unit. The prevention of silicate deposits is achieved by the stabilization of silica colloids using a polymeric antiscalant containing functional groups. The polymeric

molecules adsorb on the surface of colloids. The interaction between colloids turns repulsive such that the colloids do not coalesce and aggregate and eventually agglomerate, which is the precursor of the deposits (dispersion) (Topçu et al., 2019). The contact point between the colloid surface and the functional group of the antiscalant is a key issue. The functional group should have an affinity to the surface of the colloids. The performance of polymeric molecules originates from their chain-like structure; however, their own monomers do not show a similar performance. The performance of polymeric antiscalants depends on the molecular weight of the antiscalants and the chemistry (affinity) of functional groups interacting with target ions. The stabilization of colloids is a function of the molecular weight ( $M_w$ ) of the antiscalants (Demadis, 2005). The  $M_w$  works in a narrow range: lower  $M_w$  does not function for the antiscalating; on the other hand, however, longer  $M_w$  may cause flocculation. The molecular weight of the antiscalants employed in this study lies in the 20–50 kDa range (Topçu et al., 2017), it needs to be varied and studied in detail for the polymers employed in this research.

#### 3.4. Computational study

For atomic-scale understanding of the role of polymeric antiscalants in solubility, the interaction of molecules with sulfide (S) and antimony (Sb) ions was investigated by performing density functional theory calculations implemented in the Vienna Ab initio Simulation Package (VASP) (Kresse, 1995; Kresse and Furthmüller, 1996) by employing the plane-wave basis projector-augmented wave (PAW) method (Blochl, 1994; Kresse and Joubert, 1999). Generalized gradient approximation (GGA) in the Perdew–Burke–Ernzerhof (PBE) form was used to approximate the exchange–correlation energy (Perdew et al., 1996). To provide a reliable approximation to weak van der Waals-type forces, the GGA functional was corrected by including the DFT-D2 method of Grimme (Grimme, 2006). Spin-polarized calculations were carried out until the total energy difference between the consecutive ionic steps was less than  $10^{-5}$ . The energy of the plane-wave basis set was limited to 500 eV and the unit cell was sampled by a  $\Gamma$ -centered k-point grid of  $1 \times 1 \times 1$ . Molecular models were dealt with by constructing a cubic unit cell where the magnitude of the lattice vectors was kept to at least 15 Å to prevent the interactions between neighboring molecules. The binding energy of a single atom to a molecule was calculated by the formula  $E_{\text{Binding}} = E_{\text{Atom}} + E_{\text{Molecule}} - E_{\text{Atom+Molecule}}$ , where the terms  $E_{\text{Atom}}$ ,  $E_{\text{Molecule}}$ , and  $E_{\text{Atom+Molecule}}$  stand for the total energies of a single atom, single molecule, and a single atom-bound molecule, respectively.

Note that the binding energies are obtained for the most favorable adsorption sites obtained from the room temperature molecular dynamics calculations. However, the computation may offer a hint about the interaction of the antiscalant molecules and the target ions. In terms of full geometry optimizations, the interaction of single S and Sb atoms with various sites of the molecules are investigated to obtain the accurate binding energy. The most favorable bonding geometry of S and Sb ions is considered to be in molecules, and the calculated binding energy for each condition is represented in Fig. 7. Sb ions seem to preferentially react with acid groups of either sulfonic acid in *a* and *c* or acrylic acid in *b*. Sb approaches through the oxygen atom of the groups and interacts with the lone pairs of the oxygen. Sb has a lower binding energy so it has favourable interaction. On the other hand, S ions tend to show bonding with carbon (*a*), oxygen (*b*), and  $\text{Na}^+$  (*c*). The interaction energy was found to be higher for all three cases than that of the corresponding Sb ion. Since the complete integration of ions to the molecular structure comes by breaking the bonds between H–C and H–O atoms, the strongest interaction is obtained from poly(acrylamide-co-vinyl sulfonic acid) where the binding energies for S and Sb atoms are calculated to be 2.75 eV and 0.95 eV, respectively. Our calculations revealed the existence of additional adsorption points on poly(acrylamide-co-vinyl sulfonic acid), which results in relatively lower binding energies. Breaking the hydrogen bond in the carboxyl group, S and Sb ions bind to poly

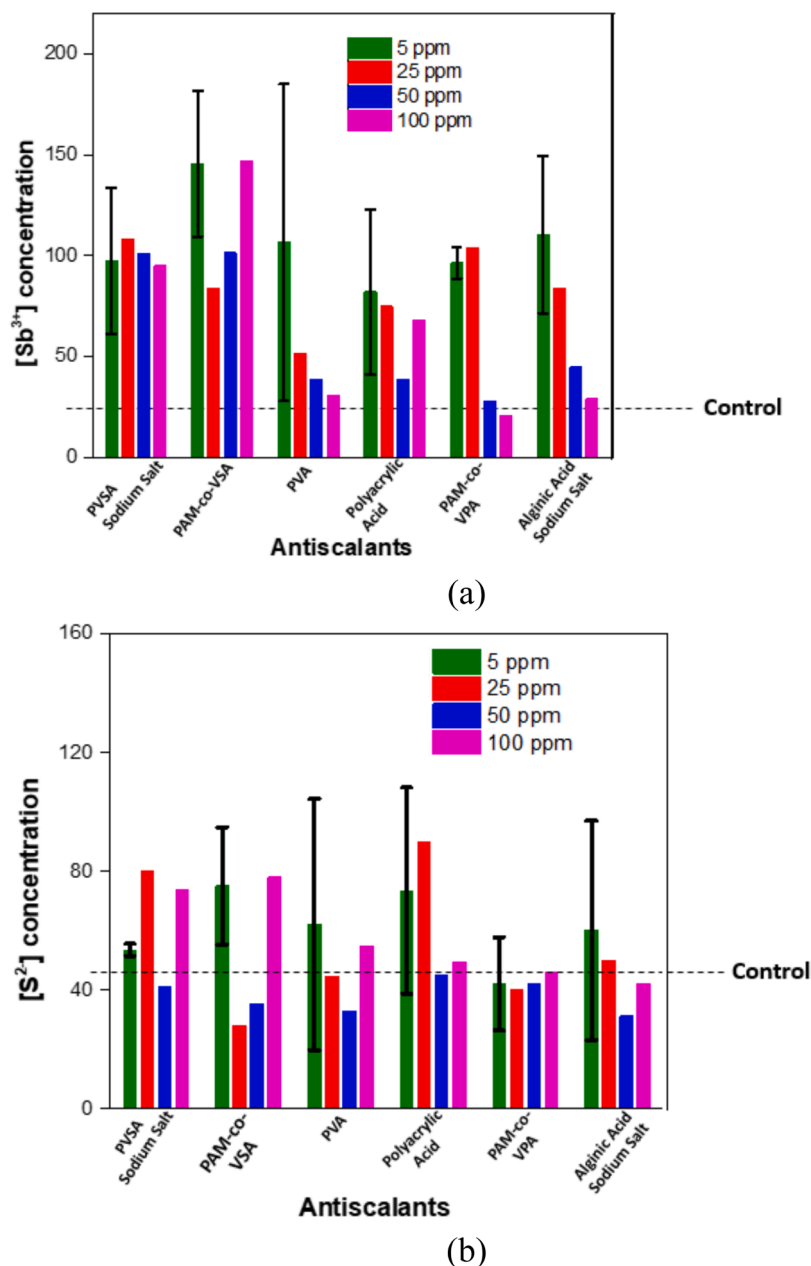


Fig. 6. The concentration of (a)  $[Sb^{3+}]$  and (b)  $[S^{2-}]$  ions in the presence of the antiscalants at various dosages. The control refers to reaction in absence of the antiscalants.

(acrylic acid) with an energy of 1.98 and 0.83 eV, respectively. In polyvinyl sulfonic acid sodium salt, ions prefer to diffuse at a point close to coordination of  $Na^+$  and O atoms with a binding energy of 1.67 and 0.65 eV, respectively.

#### 4. Conclusions

In this study, stibnite was synthesized in a pressurized reactor imitating real field conditions (135 °C and 3.5 bar). In a second step, the performance of some polymeric antiscalants marked by various functional organic groups on the mitigation of stibnite formation was examined. The dosage of the antiscalants was one of the main parameters controlling the performance of the antiscalants. All functional groups show antiscaling performance to some extent. However, the effect of the antiscalants on the concentration of Sb and S ions in solution was different. The best solubility performance was generally obtained for the smaller dosage of 5 ppm because at higher dosages the colloids

may start flocculating. Sulfonic acid-containing polymers increase the concentration of both Sb and S in the decantate solution at almost all dosages. In this sense, the usage of antiscalants containing this group will be propitious.

#### CRediT authorship contribution statement

**Emre Karaburun:** Investigation, Writing – original draft. **Yigit Sozen:** Formal analysis. **Celal Çiftçi:** Investigation. **Hasan Sahin:** Formal analysis. **Alper Baba:** Validation. **Ümit Akbey:** Investigation. **Mehmet İrfan Yeşilnacar:** Investigation. **Eray Erdim:** Investigation. **Simona Regensburg:** Validation. **Mustafa M. Demir:** Conceptualization, Validation, Writing – review & editing, Supervision.

#### Declaration of Competing Interest

The authors declare that they have no known competing financial

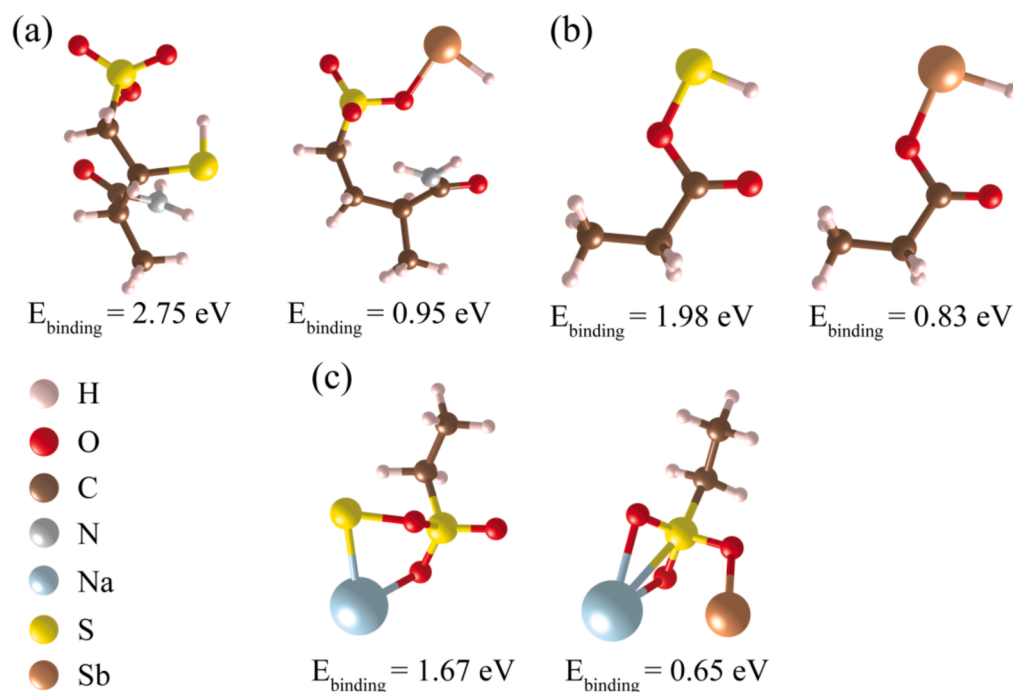
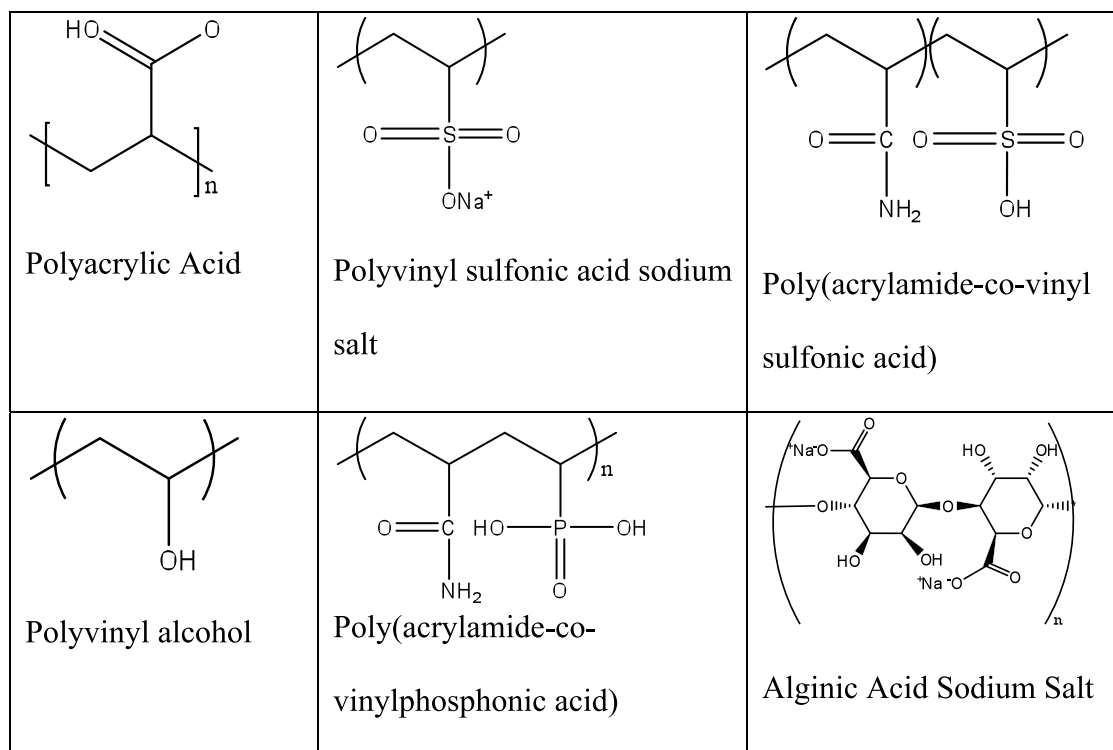


Fig. 7. The geometric structure of S and Sb bonded (a) poly(acrylamide-co-vinyl sulfonic acid), (b) poly(acrylic acid) and (c) polyvinyl sulfonic acid sodium salt molecules with the corresponding binding energies calculated.



Scheme 1. Chemical structure of the polymeric antiscalants employed in this study for the mitigation of the antimony-rich deposit.

interests or personal relationships that could have appeared to influence the work reported in this paper.

#### Acknowledgements

This project has received funding from the European Union's Horizon 2020 research and innovation program under grant agreement No

850626 (REFLECT). The authors thanks Center for Materials Research of Izmir Institute of Technology for Microscopy and Diffraction measurements. C.Ç. thanks 100/2000 CoHE PhD Scholarship Program of Council of Higher Education of Turkey (YÖK).

## References

- Andre, P., 1996. Stibnite veins and disseminations. Selected British Columbia Mineral Deposit Profiles, 2. British Columbia Ministry of Employment and Investment, Open file 1996-13, pp. 77–80.
- Azaroual, M., Kervevan, C., Durance, M.v, Durst, P., 2004. SCALE2000: reaction-transport software dedicated to thermokinetic prediction and quantification of scales applicability to desalination problems. *Desalination* 165, 409–419.
- Baba, A., Demir, M.M., Koç, G.A., Tuğcu, C., 2015. Hydrogeological properties of hyper-saline geothermal brine and application of inhibiting siliceous scale via pH modification. *Geothermics* 53, 406–412. <https://doi.org/10.1016/j.geothermics.2014.08.007>.
- Bloch, P.E., 1994. Projector augmented-wave method. *Phys. Rev. B* 50, 17953–17979.
- Brown, K., 2011. Antimony and arsenic sulfide scaling in geothermal binary plants 103–106.
- Çiçek, A., 2020. The electric power production targeted Unconventional Geothermal Systems (UGS), some conceptual designs and their thermodynamics classification. *Bull. Miner. Res. Explor.* 163, 211–228. <https://doi.org/10.19111/bulletinofmre.660706>.
- Çiftçi, C., Karaburun, E., Tonkul, S., Baba, A., Demir, M.M., Yeşilnacar, M.İ., 2020. Testing the performance of various polymeric antisalants for mitigation of Sb-rich precipitates mimicking stibnite-based geothermal deposits. *Geofluids* 2020. <https://doi.org/10.1155/2020/8867084>.
- Clearfield, A., Demadis, K.D., 2012. Metal phosphonate chemistry from synthesis to applications preface. *Metal phosphonate chemistry: from synthesis to applications*.
- Demadis, K.D., 2005. A structure/function study of polyaminoamide dendrimers as silica scale growth inhibitors. *J. Chem. Technol. Biotechnol.* 80, 630–640. <https://doi.org/10.1002/jctb.1242>.
- Demadis, K.D., Stathouloupoulou, A., 2006. Solubility enhancement of silicate with polyamine/polyammonium cationic macromolecules: Relevance to silica-laden process waters. *Ind. Eng. Chem. Res.* 45 (12).
- Demir, M.M., Baba, A., Atilla, V., Inanlı, M., 2014. Types of the scaling in hyper saline geothermal system in northwest Turkey. *Geothermics* 50, 1–9. <https://doi.org/10.1016/j.geothermics.2013.08.003>.
- Ellis, A.J., Mahon, W.A.J., 1977. *Chemistry and Geothermal Systems*. Academic Press, New York (OcoLC)609093824.
- Faucher, A., Terskikh, V.V., Wasylishen, R.E., 2014. Feasibility of arsenic and antimony NMR spectroscopy in solids: an investigation of some group 15 compounds. *Solid State Nucl. Magn. Reson.* 61–62, 54–61. <https://doi.org/10.1016/j.snmr.2014.05.005>.
- Gallup, D.L., 2002. Investigations of organic inhibitors for silica scale control in geothermal brines. *Geothermics* 32, 415–430.
- Grimme, S., 2006. Semiempirical GGA-type density functional constructed with a long-range dispersion correction. *J. Comput. Chem.* 27, 1787–1799. <https://doi.org/10.1002/jcc.20495>.
- Harmening, T., Eckert, H., Pöttgen, R., 2009. Defects in half-Heusler type antimonides ScTSb (T = Ni, Pd, Pt). *Solid State Sci.* 11, 900–906. <https://doi.org/10.1016/j.solidstatesciences.2008.12.007>.
- Hofstra, A.H., Marsh, E.E., Todorov, T.I., Emsbo, P., 2013. Fluid inclusion evidence for a genetic link between simple antimony veins and giant silver veins in the Coeur d'Alene mining district, ID and MT, USA. *Geofluids* 13, 475–493. [10.1111/gfl.12036](https://doi.org/10.1111/gfl.12036).
- Kresse, G., 1995. Ab initio molecular dynamics for liquid metals. *J. Non Cryst. Solids* 192& 193, 222–229.
- Kresse, G., Furthmüller, J., 1996. Efficient iterative schemes for ab initio total-energy calculations using a plane-wave basis set 54.
- Kresse, G., Joubert, D., 1999. From ultrasoft pseudopotentials to the projector augmented-wave method 59, 1758–1775.
- Krupp, E., 1988. YXX-M15 Copyright C 1988 52.
- Li, C., Yang, X., Liu, Y., Zhao, Z., Qian, Y., 2003. Growth of crystalline Sb<sub>2</sub>S<sub>3</sub> nanorods by hydrothermal method. *J. Cryst. Growth* 255, 342–347. [https://doi.org/10.1016/S0022-0248\(03\)01266-1](https://doi.org/10.1016/S0022-0248(03)01266-1).
- Miller, M., 1973. United States mineral sources . Geological Survey Professional Paper 820.
- Perdew, J.P., Burke, K., Ernzerhof, M., 1996. Generalized gradient approximation made simple 77, 3865–3868.
- Reyes, A.G., Trompeter, W.J., Britten, K., Searle, J., 2002. Mineral deposits in the Rotokawa geothermal pipelines, New Zealand 119, 215–239.
- Stauffer, R.E., Thompson, J.M., 1984. *Arsenic and Antimony in Geothermal Waters of Yellowstone National Park*, 48. Wyoming, USA, pp. 2547–2561.
- Topçu, G., Çelik, A., Baba, A., Demir, M.M., 2017. Design of polymeric antisalants based on functional vinyl monomers for (Fe, Mg) silicates. *Energy Fuels* 31, 8489–8496. <https://doi.org/10.1021/acs.energyfuels.7b01221>.
- Topcu, G., Çelik, A., Kandemir, A., Baba, A., Sahin, H., Demir, M.M., 2019. Increasing solubility of metal silicates by mixed polymeric antisalants. *Geothermics* 77, 106–114. <https://doi.org/10.1016/j.geothermics.2018.09.002>.
- Ubalini, S., Veglio, F., Fornari, P., Abbruzzese, C., 2000. Process flow-sheet for gold and antimony recovery from stibnite. *Hydrometallurgy* 57, 187–199.
- Williams-Jones, A.E., Nohmand, C., 1997. Controls of mineral parageneses in the system Fe-Sb-S-O. *Econ. Geol.* 92, 308–324.
- Wilson, N., Webster-Brown, J., Brown, K., 2007. Controls on stibnite precipitation at two New Zealand geothermal power stations. *Geothermics* 36, 330–347. <https://doi.org/10.1016/j.geothermics.2007.04.001>.